An analytical study on the combination of profile relief and lead crown minimizing transmission error in narrow-faced helical gears

Jérôme Bruyère, P. Velex, B. Guilbert, D.R. Houser

An analytical study on the combination of profile relief and lead crown minimizing transmission error in narrow-faced helical gears.

BRUYERE, J. [a], VELEX, P. [a], GUILBERT B. [a] and HOUSER, D. R. [b]

Revised version

February 2019

[a] Univ Lyon, INSA-Lyon, CNRS UMR5259, LaMCoS, F-69621, France

[b]The Ohio State University, Columbus, OH, USA

* Corresponding author: Philippe.Velex@insa-lyon.fr

Tel. +33 4 72 43 84 51

Fax. +33 4 78 89 09 80

Submitted to Mechanism and Machine Theory.

Abstract

Some original analytical developments and results on the formulation of transmission error in solid spur and helical gears are presented, which lead to closed-form formulae defining the optimum combinations of profile relief and lead crown minimising the time-variation amplitudes of transmission error. Extensive comparisons with the results of benchmark software codes prove that the analytical findings are sound and can be used at the initial design stage to define optimum modifications with minimum effort. Some qualitative general trends can also be derived. In particular, it is shown that optimum tooth modifications depend on a limited number of dimensionless parameters, namely the profile and face contact ratios, the normalised depth and extent of profile modifications along with the normalised lead crown amplitude. The influence of the latter is found to strongly depend on a specific function of face contact ratio, which controls the displacement of optimum profile relief either towards the smaller or larger depths of modification at tooth tips. Finally, the analytical formulae (and the numerical simulations) indicate that the optimum modifications are approximately located along a line segment in the relief versus crown amplitude plane.

Keywords: gears; transmission error; profile modifications; lead crown; analytical formulae; face contact ratio

1 - Introduction

Profile relief and lead modifications on gear teeth are necessary whenever significant power is transmitted in order to avoid, i) abrupt load variations at engagement and recess (working interferences) and, ii) edge contacts in the presence of misalignments [1-2]. Profile modifications usually consist in removing material near the tip or root of the teeth and are often linear or parabolic in the profile direction (or MAAG-type diagrams). Lead modifications can be limited to tooth edges (chamfers for instance) or cover the entire tooth width. Beyond the optimization of tooth load pattern, it has been demonstrated that tooth shape modifications can also significantly alter the noise and vibration levels which, to a large extent, are correlated with the amplitudes of the time-variations of quasi-static transmission error under load (TE_S). Many papers, only a few of which can be cited here [3-10], have been published on this topic. They mainly rely on massive numerical simulations including systematic sweeps over modification parameters [11-20] or heuristic optimization methods such as genetic algorithms [21-24]. The vast majority of the results, however, show that, regardless of gear macro-geometry, there exist families of optimal modifications, which minimize the time-variations of TE_S at a given load. Based on analytical results [25-28], closed-form formulae have been proposed which give the optimum dimensionless depth and length of modification for symmetric linear profile relief defining so-called Master Curves [26] valid for a range of spur and helical gears and loads. Comparisons with benchmark software codes are satisfactory and, as opposed to numerical simulation results, some general trends can be derived about the influence of gear geometry, profile relief parameters and loads.

The objective of this paper is to extend the closed-form definition of optimal profile relief to the case of combined profile and lead modifications. It is demonstrated that, for

moderate crown amplitudes (typically less than the average mesh deflection), a simple dimensionless formula can be derived which gives a good estimate of the combinations of linear profile relief and parabolic lead crown minimizing transmission error for a variety of gears and a range of loads. The specific influence of the face contact ratio is highlighted and it is shown that, depending on its value, contrasted influence of lead crown on TEs can be expected from detrimental to beneficial including cases for which, nearly no influence can be reported.

Nomenclature

b : contact width

$b_{1,2}$: face width of pinion, of gear

B^*: dimensionless lead crown amplitude *(normalized with respect to the average static mesh deflection* δ_m*).*

$e^*(M) = e_E^*(M) + e_B^*(M)$

$e_E^*(M)$, dimensionless profile relief (sum of the pinion and gear normal deviations with respect to ideal flanks at any generic contact point M)*(normalized with respect to the average static mesh deflection* δ_m*)*

$e_B^*(M)$, dimensionless lead crown modification (sum of the pinion and gear normal deviations with respect to ideal flanks at any generic contact point M)*(normalized with respect to the average static mesh deflection* δ_m*)*

E^*: dimensionless depth of profile relief at tooth tips *(normalized with respect to the average static mesh deflection* δ_m*)* .

F_N ; total normal mesh force.

$h_{a1,a2}$: addendum coefficient on pinion, on gear

$h_{f1,f2}$: dedendum coefficient on pinion, on gear

$k_m = \int_0^1 \int_{M \in L_0(\tau)} k(M)\, dM\, d\tau$ average mesh stiffness in the absence of tooth shape deviations and errors (*integrated over the theoretical contact length* $L_0(\tau)$) .

k_0: constant or average mesh stiffness per unit of contact length.

$k(M)$, mesh stiffness per unit of contact length at M .

$\hat{k}(M)$, dimensionless mesh stiffness per unit of contact length at M *(normalized with respect to the average mesh stiffness* k_m*).*

$\hat{k}(\tau, \mathbf{X}_S)$, dimensionless time-varying, non-linear mesh stiffness function *(normalized with respect to the average mesh stiffness* k_{m0}*).*

$L(\tau, \mathbf{X}_S), L_0(\tau)$: time-varying (possibly non-linear) contact length, theoretical contact length.

m_0 : module

M_{00}: point at the entry of the contact zone at τ=0 (Figure 4).

$\mathbf{n}$: outward unit normal vector with respect to pinion flanks.

$NLTE(\tau)$: no-load transmission error.

P_{bt} : apparent base pitch.

T_m : mesh period.

T_1, T_2 : limits of base plane (Figure 4)

$TE_S(\tau), TE_S^*(\tau)$: actual and dimensionless quasi-static transmission error under load *(normalized with respect to the average static mesh deflection* δ_m*)*

$x_{1,2}$: profile shift coefficient on pinion, on gear

z, z^* : axial and dimensionless axial coordinates ($z^* = z / b$)

Z_1, Z_2 : tooth number on pinion, on gear

α_0 : pressure angle

β_0, β_b: helix angle, base helix angle

$\delta_m = \frac{F_N}{k_m}$: static mesh deflection with average mesh stiffness for ideal gears

ε_α : theoretical profile contact ratio (with no contact length reduction)

$\varepsilon'_\alpha = (1-2\lambda)\varepsilon_\alpha$: actual profile contact ratio

ε_β : face contact ratio (overlap contact ratio)

$\Gamma = \frac{\ell_r}{\varepsilon_\alpha P_{ba}}$: dimensionless extent of profile modification where ℓ_r is the length (or extent) of relief measured in the base plane

$\Gamma_L = 1 - 1/\varepsilon_\alpha$, dimensionless extent of modification for the so-called long relief

λ , contact length reduction factor *(accounts for delayed engagement and premature end of recess)*

$\eta(\varepsilon_\beta) = \frac{1}{(\pi\varepsilon_\beta)^2} - \frac{1}{(\pi\varepsilon_\beta)\tan(\pi\varepsilon_\beta)} - \frac{1}{3}$, see Figure 5

Ω_1 , pinion rotational speed

$\tau = \frac{t}{T_m}$, dimensionless time

$\hat{A} = \frac{A}{k_m}$, for any generic variable *A*; normalization with respect to the nominal average mesh stiffness $k_m = \int_0^1 \int_{M \in L_0(\tau)} k(M)\, dM\, d\tau$ in the absence of tooth shape deviations and errors.

$A^* = \frac{A}{\delta_m}$, for any generic variable *A* such that $\delta_m = \frac{F_N}{k_m}$ (F_N *is the normal mesh force*)

2 - Theory

2-1 Profile and lead modifications

In this paper, combinations of profile and lead modifications are considered which comprise a) symmetric linear relief on pinion and gear tips or roots and, b) a parabolic crown in the lead direction on the pinion and/or the gear. The geometries of the corresponding tooth shape modifications are represented in Figs. 1 and 2.

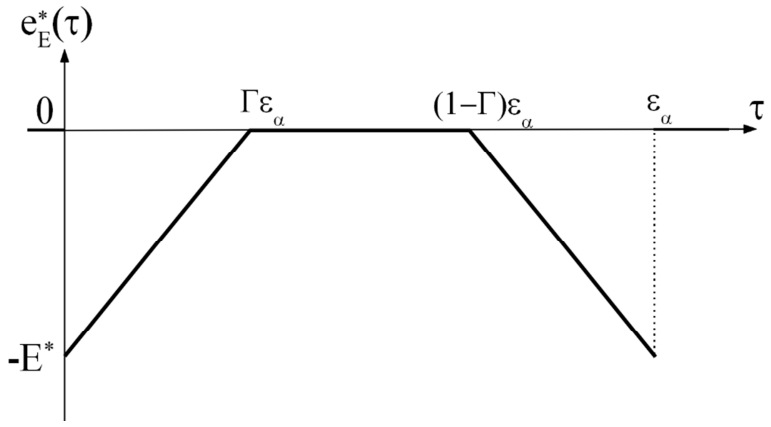

Figure 1 – Definition of tooth profile modifications (linear symmetric relief)

Following a tooth pair from its engagement to its end of recess, the composite profile relief on the pinion and gear tips (Fig. 1) can be expressed in terms of the dimensionless coordinate along the line of action $\tau = x / P_{bt}$ (P_{bt} is the apparent base pitch) as:

$$e_E^*(\tau) = \begin{cases} -E^*\left(\dfrac{-\tau}{\Gamma\varepsilon_\alpha}+1\right) & 0 \le \tau \le \Gamma\varepsilon_\alpha \\ -E^*\left(\dfrac{\tau}{\Gamma\varepsilon_\alpha}-\dfrac{1}{\Gamma}+1\right) & (1-\Gamma)\varepsilon_\alpha \le \tau \le \varepsilon_\alpha \\ 0 & \text{otherwise} \end{cases} \qquad (1)$$

where

$\Gamma\varepsilon_\alpha$ is the dimensionless extent of modification measured on the line of action,

$E^* = \dfrac{E}{\delta_m}$, E is the actual depth of modification at tooth tip and $\delta_m = \dfrac{F_N}{k_m}$ is the average mesh deflection (F_N is the normal mesh force and k_m, the average mesh stiffness for perfect, unmodified tooth flanks).

The trace of the parabolic crown shown in Fig. 2 is expressed in terms of the dimensionless axial coordinate z^* and dimensionless crowning amplitude $B^* = \dfrac{B}{\delta_m}$ as:

$$e_B^*(z^*) = -B^*\left(1-4z^*+4z^{*2}\right) \quad 0 \le z^* \le 1, \; z^* = z/b \qquad (2)$$

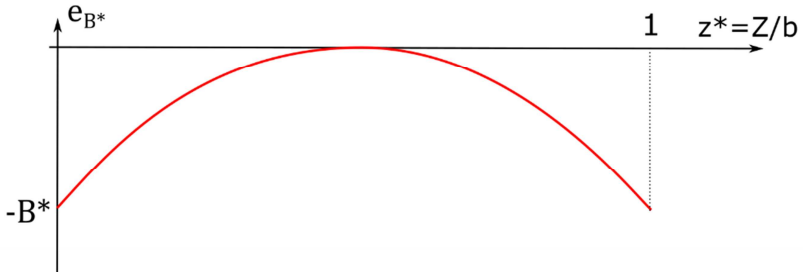

Figure 2 – Lead modification (parabolic crown)

The resulting total tooth surface modification is the sum of the deviations generated by profile relief and lead crowning (Figure 3) and reads:

$$e^*\left(\tau, z^*\right) = e_E^*\left(\tau\right) + e_B^*\left(z^*\right) \qquad (3)$$

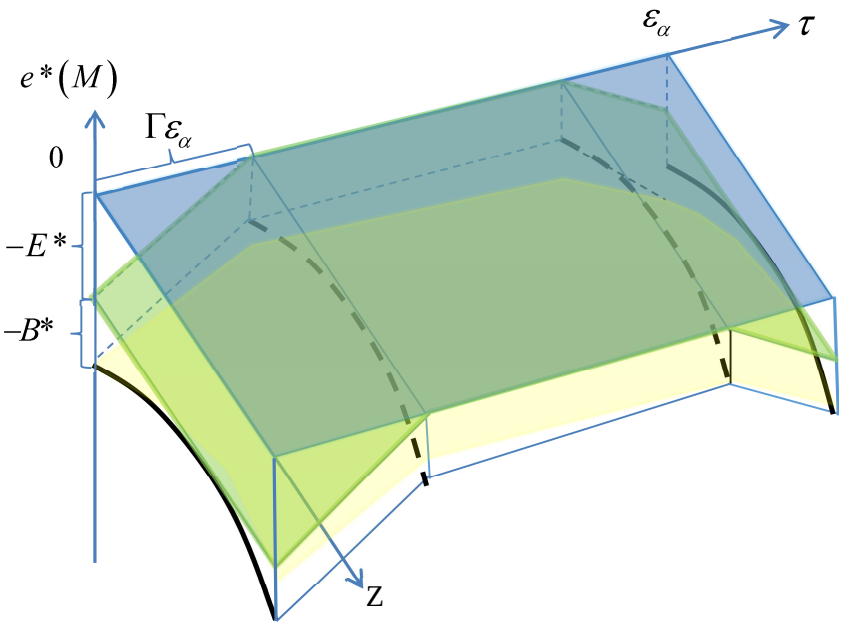

Figure 3 – Composite tooth shape deviations (superposition of profile and lead modifications)

2-2 Transmission error,

Following [25], the dimensionless quasi-static transmission error $TE_S^*\left(\tau\right)$ for spur and helical gears with profile and lead modifications can be expressed as:

$$\cos\beta_b \, TE_S^*\left(\tau\right) = \frac{1 - I_{kE} - I_{kB}}{I_k} \qquad (4)$$

with:

$$I_{kE} = \int_{M\in(L)} \hat{k}(M)\, e_E^*(M)\, dM \,,$$

$$I_{kB} = \int_{M\in(L)} \hat{k}(M)\, e_B^*(M)\, dM$$

$I_k = \int_{M \in (L)} \hat{k}(M)\, dM$ which represents the mesh stiffness function

$\hat{k}(M) = \dfrac{k(M)}{k_m}$, dimensionless mesh stiffness per unit contact length at point *M*

The integrals over the instant length of contact L above can be simplified to a large extent, if one considers a constant mesh stiffness per unit contact length $k(M) \approx k_0$ which leads to the following expressions (Fourier series) [25-27]:

$$I_{kE} = -\frac{E^*(\Gamma-\lambda)^2}{\Gamma}\left[1-\sum_{k=1}^{\infty}\Omega_{kE}\cos\left[\pi k\left(\varepsilon_\alpha+\varepsilon_\beta-2\tau\right)\right]\right] \quad (5)$$

$$I_{kB} = -B^*(1-2\lambda)\left[\frac{1}{3}+\sum_{k=1}^{\infty}\Omega_{kB}\cos\left[\pi k\left(\varepsilon_\alpha+\varepsilon_\beta-2\tau\right)\right]\right] \quad (6)$$

$$I_k = (1-2\lambda)\left[1+\sum_{k=1}^{\infty}\Omega_k\cos\left[\pi k\left(\varepsilon_\alpha+\varepsilon_\beta-2\tau\right)\right]\right] \quad (7)$$

with

$$\Omega_{kE} = \frac{2}{\Gamma-\lambda}\mathrm{Sinc}\left[k\varepsilon_\beta\right]\left\{(2\lambda-1)\mathrm{Sinc}\left[k(1-2\lambda)\varepsilon_\alpha\right]+(1-\Gamma-\lambda)\mathrm{Sinc}\left[k\varepsilon_\alpha(1-\Gamma-\lambda)\right]\mathrm{Sinc}\left[k\varepsilon_\alpha(\Gamma-\lambda)\right]\right\} \quad (8)$$

$$\Omega_{kB} = 2\mathrm{Sinc}\left[k(1-2\lambda)\varepsilon_\alpha\right]\left[\left(1-\frac{2}{(\pi k\varepsilon_\beta)^2}\right)\mathrm{Sinc}\left[k\varepsilon_\beta\right]+\frac{2\cos\left[\pi k\varepsilon_\beta\right]}{(\pi k\varepsilon_\beta)^2}\right] \quad (9)$$

$$\Omega_k = 2\,\mathrm{Sinc}\left[k(1-2\lambda)\varepsilon_\alpha\right]\mathrm{Sinc}\left[k\varepsilon_\beta\right] \quad (10)$$

"Sinc" is the classic sine cardinal function defined as $\mathrm{Sinc}(x) = \dfrac{\sin(\pi x)}{\pi x}$

λ is the contact length reduction parameter possibly induced by tooth shape modifications such that the actual profile contact ratio is $(1-2\lambda)\varepsilon_\alpha$ upon assuming symmetry between the meshing conditions at engagement and the end of recess (*developed in section 2-3 below*).

2-3 Approximate contact length reduction

In what follows, the following hypotheses are employed in order to estimate analytically the contact area reduction in the base plane possibly brought about by profile relief and crowning:

a) Moderate crown amplitudes are considered so that the width of contact remains approximately equal to the theoretical contact width *b*,

b) In the profile direction, contact length reductions can be characterised by using a single parameter λ defining the positions where the first and final contacts occur in the base plane (Figure 4) (symmetry is assumed between engagement and the end of recess).

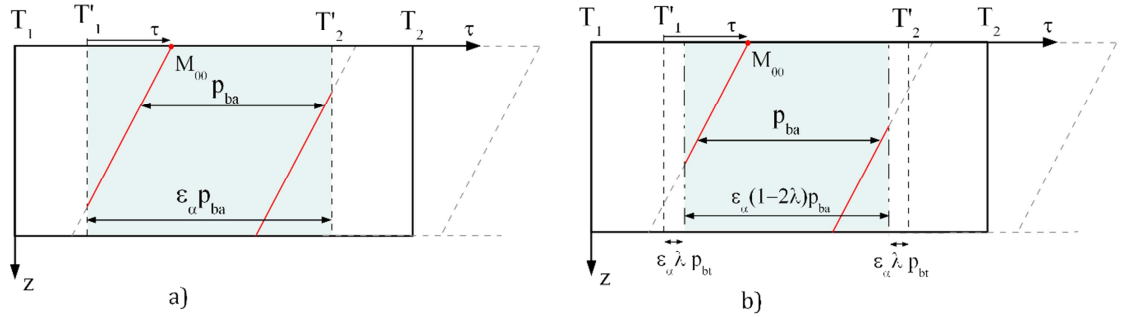

Figure 4: a) Nominal meshing window and b) effective meshing window

Based on the developments in Annex 1, the approximate limits of the active base plane, which are valid as long as $\varepsilon_\beta > 0.4$, are obtained by solving the following equation:

$$\lambda^2 - \lambda + \Gamma\left(1 - \Gamma - \frac{1}{E^*}\right) = 0 \qquad (11)$$

whose only admissible solution ($\lambda < 0.5$) is:

$$\lambda \approx \frac{1 - \sqrt{1 - 4\Gamma\left(1 - \Gamma - \frac{1}{E^*}\right)}}{2} \qquad (12)$$

It can be noticed that, in these conditions, the reduction in contact length is independent of the crown amplitude and that the limit of no contact reduction ($\lambda = 0$) is given by

$$1 - \Gamma \approx \frac{1}{E^*} \qquad (13)$$

2-4 Time-variations of transmission error

Based on the developments presented in Annex 2, the variance (or squared RMS) of the quasi-static transmission error under load can be approximated as:

$$RMS^2\left(TE_S^*\right) \approx \frac{1}{2(1-2\lambda)^2\cos^2\beta_b}\sum_k\left(\Omega_k\left(1+\frac{E^*(\Gamma-\lambda)^2}{\Gamma}+\frac{(1-2\lambda)B^*}{3}\right)+\frac{E^*(\Gamma-\lambda)^2}{\Gamma}\Omega_{kE}-(1-2\lambda)B^*\Omega_{kB}\right)^2$$

$$=\frac{2}{(1-2\lambda)^2\cos^2\beta_b}\sum_{k=1}^{\infty}\left\langle\left\{\ \mathrm{Sinc}\left(k(1-2\lambda)\varepsilon_\alpha\right)\mathrm{Sinc}\left(k\varepsilon_\beta\right)\frac{1}{1-2\lambda}+\right.\right.$$

$$E^*\left(1-\frac{\lambda}{\Gamma}\right)\frac{1-\Gamma-\lambda}{1-2\lambda}\mathrm{Sinc}\left(k\varepsilon_\beta\right)\left[\mathrm{Sinc}\left(k\varepsilon_\alpha(1-\Gamma-\lambda)\right)\mathrm{Sinc}\left(k\varepsilon_\alpha(\Gamma-\lambda)\right)\text{-}\mathrm{Sinc}\left(k(1-2\lambda)\varepsilon_\alpha\right)\right]$$

$$\left.\left.-2B^*\mathrm{Sinc}\left(k(1-2\lambda)\varepsilon_\alpha\right)\left[\left(\frac{1}{3}-\frac{1}{\left(\pi k\varepsilon_\beta\right)^2}\right)\mathrm{Sinc}\left(k\varepsilon_\beta\right)+\frac{\cos\left(\pi k\varepsilon_\beta\right)}{\left(\pi k\varepsilon_\beta\right)^2}\right]\right\rangle^2 \qquad (14)$$

The expression above can be simplified for integer $\varepsilon_\beta \neq 0$ leading to:

$$RMS^2\left(TE_S^*\right)=\frac{8B^{*2}}{(1-2\lambda)^2\cos^2\beta_b}\sum_{k=1}^{\infty}\left[\frac{Sinc\left(k(1-2\lambda)\varepsilon_\alpha\right)}{\pi^2{\varepsilon_\beta}^2k^2}\right]^2 \qquad (15)$$

From a practical perspective, it can be observed that the time-variations of the dimensionless transmission error function TE_S^* depend on a limited number of parameters, which are: a) ε_α and ε_β characterising gear geometry and, b) the dimensionless profile and lead modifications parameters E^*, Γ and B^*. It can also be noticed that, for integral overlap ratios ε_β, crowning can only increase the time-variation amplitudes of transmission error.

3 – Minimisation of the RMS of transmission error – Master curves

Examining the various components in (14) for non-integer ε_β, it can be noticed that the corresponding Fourier series converges rapidly since it consists of terms proportional to $\frac{1}{k^n}$ with $n \geq 4$, so that the first order approximation ($k=1$) is already a good estimate of the RMS of transmission error. In these conditions, the actual minimisation of the time-variations of TE_S^* is replaced by finding the tooth shape modification parameters that cancel the first order terms in (14). By so doing, the following expression of the RMS of transmission error will be used:

$$RMS^2\left(TE^*s\right)\cong\frac{2}{\cos^2\beta_b}\Bigg\langle\ \mathrm{Sinc}\left(\left(1-2\lambda\right)\varepsilon_\alpha\right)\frac{1}{1-2\lambda}+$$
$$E^*\left(1-\frac{\lambda}{\Gamma}\right)\frac{1-\Gamma-\lambda}{1-2\lambda}\left[\mathrm{Sinc}\left(\varepsilon_\alpha\left(1-\Gamma-\lambda\right)\right)\mathrm{Sinc}\left(\varepsilon_\alpha\left(\Gamma-\lambda\right)\right)\text{-}\mathrm{Sinc}\left(\left(1-2\lambda\right)\varepsilon_\alpha\right)\right] \qquad (16)$$
$$-2B^*\mathrm{Sinc}\left(\left(1-2\lambda\right)\varepsilon_\alpha\right)\left[\left(\frac{1}{3}-\frac{1}{\left(\pi\varepsilon_\beta\right)^2}\right)+\frac{1}{\left(\pi\varepsilon_\beta\right)\tan\left(\pi\varepsilon_\beta\right)}\right]\Bigg\rangle^2$$

3-1 Cases with reduction in actual contact length or profile contact ratio ($\lambda>0$)

The approximate expression of the RMS of transmission error (16) can be simplified by introducing (11) (re-written as $E^*\left(1-\frac{\lambda}{\Gamma}\right)\left(1-\Gamma-\lambda\right)=1$) thus leading to:

$$RMS^2\left(TE^*s\right)\cong\frac{2}{\cos^2\beta_b}\Bigg\langle\ \frac{1}{1-2\lambda}\left[\mathrm{Sinc}\left(\varepsilon_\alpha\left(1-\Gamma-\lambda\right)\right)\mathrm{Sinc}\left(\varepsilon_\alpha\left(\Gamma-\lambda\right)\right)\right] \qquad (17)$$
$$+2B^*\eta\left(\varepsilon_\beta\right)\mathrm{Sinc}\left(\left(1-2\lambda\right)\varepsilon_\alpha\right)\Bigg\rangle^2$$

with

$\eta\left(\varepsilon_\beta\right)=\frac{1}{\left(\pi\varepsilon_\beta\right)^2}-\frac{1}{\left(\pi\varepsilon_\beta\right)\tan\left(\pi\varepsilon_\beta\right)}-\frac{1}{3}$ which is represented in Figure 5.

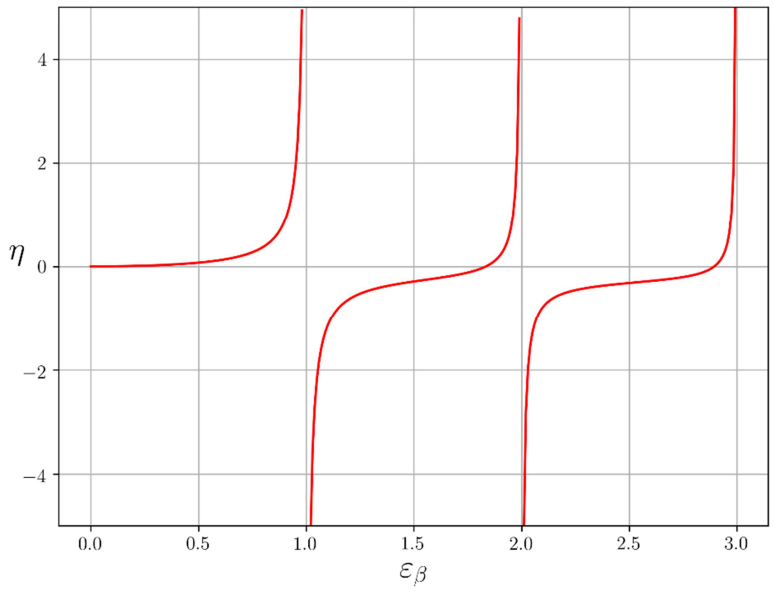

Figure 5: Function $\eta(\varepsilon_\beta)$ versus ε_β

The set of profile and lead modification parameters E^*, Γ and B^* minimising the time-variations of the quasi-static transmission error under load is therefore the solution of the following two equations:

$$\mathrm{Sinc}\left(\varepsilon_\alpha(1-\Gamma-\lambda)\right)\mathrm{Sinc}\left(\varepsilon_\alpha(\Gamma-\lambda)\right)+2B^*\eta(\varepsilon_\beta)(1-2\lambda)\mathrm{Sinc}\left((1-2\lambda)\varepsilon_\alpha\right)=0 \tag{18}$$

$$E^*\left(1-\frac{\lambda}{\Gamma}\right)(1-\Gamma-\lambda)=1 \tag{19}$$

After developing the *Sinc* functions and simplifying, (18) is re-formulated as:

$$H(\lambda)+2B^*\eta(\varepsilon_\beta)=0 \tag{20}$$

with

$$H(\lambda)=\frac{E^*}{\Gamma\pi\varepsilon_\alpha}\frac{\sin\left(\pi\varepsilon_\alpha(1-\Gamma-\lambda)\right)\sin\left(\pi\varepsilon_\alpha(\Gamma-\lambda)\right)}{\sin\left(\pi\varepsilon_\alpha(1-2\lambda)\right)} \tag{21}$$

Denoting λ_0 , the value of the contact length reduction factor such that $H(\lambda_0)=0$, it can be observed, based on Figure 5, that the product $B^*\eta(\varepsilon_\beta)$ is a small quantity as long as ε_β is not too close to integral values. A solution to (20) can therefore be sought by using the following first order development:

$$H(\lambda) \approx H(\lambda_0)+(\lambda-\lambda_0)\left[\frac{dH(\lambda)}{d\lambda}\right]_{\lambda=\lambda_0} \tag{22}$$

whose only physically admissible solution λ_0 for $\varepsilon_\alpha<2$ is:

$$\sin\left(\pi\varepsilon_\alpha(1-\Gamma-\lambda_0)\right)=0 \tag{23}$$

Hence

$$\lambda_0=1-\Gamma-\frac{1}{\varepsilon_\alpha} \tag{24}$$

After some developments, it is found that:

$$\left[\frac{dH(\lambda)}{d\lambda}\right]_{\lambda=\lambda_0}=-\frac{E^*}{\Gamma} \tag{25}$$

so that:

$$H(\lambda) \approx -(\lambda-\lambda_0)\frac{E^*}{\Gamma} \qquad (26)$$

and

$$\lambda = \lambda_0 + 2\frac{\Gamma}{E^*}B^*\eta(\varepsilon_\beta) = 1-\Gamma-\frac{1}{\varepsilon_\alpha}+2\frac{\Gamma}{E^*}B^*\eta(\varepsilon_\beta) \qquad (27)$$

which, when re-injected into (19) leads to:

$$\frac{E^*}{\Gamma\varepsilon_\alpha}\left(2\Gamma-1+\frac{1}{\varepsilon_\alpha}-2\frac{\Gamma}{E^*}B^*\eta(\varepsilon_\beta)\right)\left(1-2\varepsilon_\alpha\frac{\Gamma}{E^*}B^*\eta(\varepsilon_\beta)\right)=1 \qquad (28)$$

Finally, an explicit form of the set of profile and lead modifications can be obtained considering that $\left[\frac{\Gamma}{E^*}B^*\eta(\varepsilon_\beta)\right]^2 << \frac{\Gamma}{E^*}B^*\eta(\varepsilon_\beta)$ as:

$$E^* \approx \frac{\Gamma\varepsilon_\alpha}{2\Gamma-1+\frac{1}{\varepsilon_\alpha}}\left[1+2B^*\eta(\varepsilon_\beta)\left(2\Gamma-1+\frac{2}{\varepsilon_\alpha}\right)\right] \qquad (29)$$

Interestingly, (29) corresponds to the formula obtained for profile relief in [26-27] multiplied by a lead crown correcting factor $2\eta(\varepsilon_\beta)\left(2\Gamma-1+\frac{2}{\varepsilon_\alpha}\right)$ such that when $B^*=0$ (no crowning), the equation reduces to the Master Curve equation for profile relief. It can therefore be inferred that the influence of a position-varying mesh stiffness per unit contact length could be introduced, as for profile relief only, via the correcting term introduced in [26], thus leading to the final equation for optimum tooth profile and lead modifications:

$$E^* \approx \frac{\Gamma\varepsilon_\alpha}{2\Gamma-1+\frac{1}{\varepsilon_\alpha}}\left[1-0.3C_f\right]\left[1+2B^*\eta(\varepsilon_\beta)\left(2\Gamma-1+\frac{2}{\varepsilon_\alpha}\right)\right] \qquad (30)$$

with

$C_f = 6\Gamma(-5\Gamma+2\Gamma_L)+6(3\Gamma-\Gamma_L)-1$ for $\frac{\Gamma_L}{2} < \Gamma \le \Gamma_L$

$\Gamma_L = 1-\frac{1}{\varepsilon_\alpha}$ which corresponds to so-called long relief according to [3]

3-2 Cases with no reduction in actual contact length (or profile contact ratio) ($\lambda = 0$)

Using (16) and setting $\lambda = 0$ directly lead to the following equation:

$$E^* = \frac{1 + 2B^*\eta(\varepsilon_\beta)}{(1-\Gamma)\left[1 - Sinc(\varepsilon_\alpha(1-\Gamma))\,Sinc(\varepsilon_\alpha\Gamma)/Sinc(\varepsilon_\alpha)\right]} \tag{31}$$

from which, the expression of the optimal tooth modifications is derived as for (30) by introducing a correcting function for position- (time-) varying mesh stiffness per unit contact length [26] as:

$$E^* = \frac{1 + 2B^*\eta(\varepsilon_\beta)}{(1-\Gamma)\left[1 - Sinc(\varepsilon_\alpha(1-\Gamma))\,Sinc(\varepsilon_\alpha\Gamma)/Sinc(\varepsilon_\alpha)\right]}\left(1 - 0.3C_f^*\right) \tag{32}$$

with

$$C_f^* = -18\Gamma_L^2 + 12\Gamma_L - 1 \text{ if } \Gamma > \Gamma_L$$
$$C_f^* = C_f \text{ otherwise}$$

3-3 Synthesis

The combination of (30) and (32) finally makes it possible to estimate the combinations of profile and lead modifications minimising transmission error over the entire range of profile relief parameters and for crown amplitudes that do not exceed the average mesh deflection. Based on (13), the respective areas where formulae (30) or (32) hold are visualized in the (E^*, Γ) plane as shown in Figure 6 (remembering that the frontier defined by (13) is independent of the crown amplitude). It can be noticed that when $\Gamma = \Gamma_L = 1 - \frac{1}{\varepsilon_\alpha}$ (long relief), the solutions from (30) and (32) are identical (the two curves always intersect at this point). The transition between (30) and (32) is defined by the condition $\lambda = 0$, which using (13), is expressed under the form $\Gamma = 1 - \frac{1}{E^*}$ and corresponds to the dotted curve in Fig. 6 separating the two solution domains. Continuity between the solutions given by the two equations (30) and (32) is not ensured and, strictly speaking, the optimum modifications cannot be represented by a unique curve. However, an approximate curve can be defined by keeping the results of (32) for extents of modifications above Γ_L (a limit beyond which it is not interesting to go) and solutions from (30) for $\Gamma < \Gamma_L$ (corresponding to the vast majority of the cases in practice). This approximation is used throughout the paper in what follows.

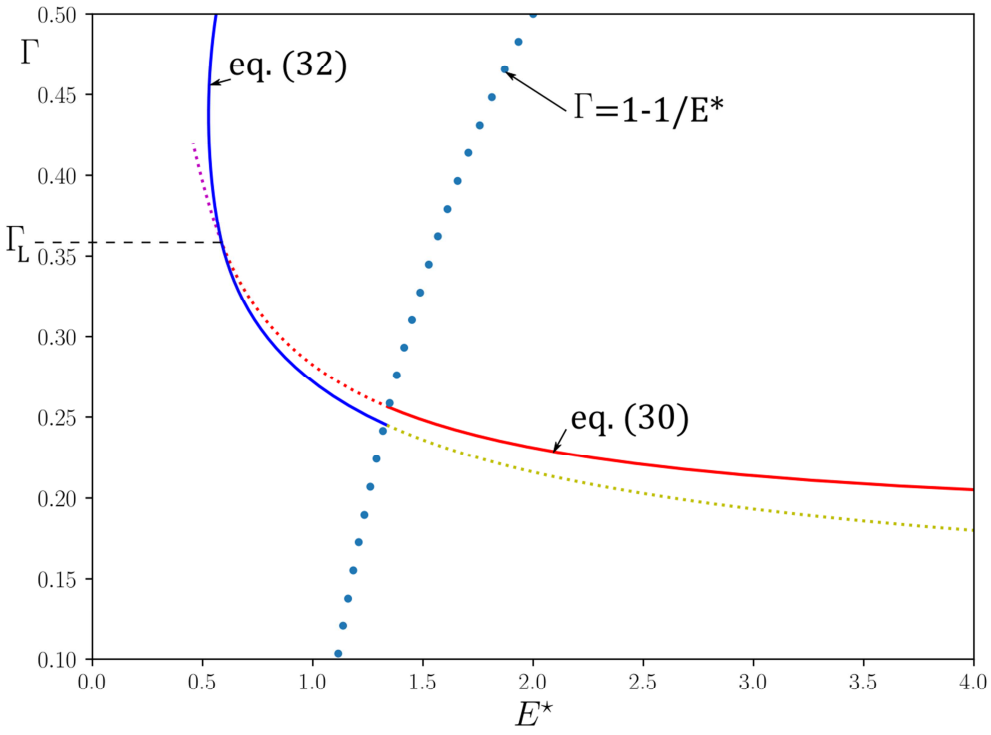

Figure 6 – Solution domains for optimum tooth shape modifications.

Physically speaking, it transpires from the formulae in (30) and (32) that, rather than the sole crown amplitude, the relevant parameter is the product $B^{*}\eta\left(\varepsilon_{\beta}\right)$ combining lead crown amplitude and face contact ratio ε_{β}. Since $\eta\left(\varepsilon_{\beta}\right)$ can either be positive or negative depending on ε_{β} (see Figure 5), contrasted results in terms of the influence of lead crown on 'optimal' tooth shape modifications are expected. In particular, the optimum curve can either move towards larger or smaller profile relief amplitudes when a range of face contact ratios is considered.

4 – Elements of validation

The proposed formulae (30) and (32) rely on a number of hypotheses (the rectangular shape of the contact area in the base plane, negligible higher-order terms in Fourier series and Taylor expansions, etc.) whose influence on the result quality needs to be assessed. To this end, extensive numerical simulations have been performed using:

a- A lumped parameter model (VSA) [8], [18] and a comprehensive hybrid 3D model [29], [30] (Figure 7) combining two condensed sub-structures with 20-node brick FE for the structural parts (pinion and gear bodies, shafts) but with the same mesh interface model using:

- a time-varying, non-linear Winkler foundation model for the mesh interface based on the analytical formulae of Weber and Banaschek [31],
- distributed time-varying initial separations to simulate tooth shape deviations [8]

b- The benchmark software code LDP [32-34] developed at the Ohio State University which is widely used in industry.

The main objective is to compare the optimum tooth modifications obtained by numerical simulations after systematic sweeps over the relief and crown parameters with the results derived from the analytical formulae (30) and (32). Several solid gear sets have been tested whose geometrical characteristics are listed in Table 1. Experimental results over sufficiently broad ranges of profiles and lead modifications have not been found in the literature so that direct comparisons between experimental and numerical master curves are not possible. However, both simulation codes have been validated based on numerous test rig measurements [35-36] and are considered as representative of actual gear behaviour.

4-1 VSA results

Figures 7 and 8 show examples of the optimum zones in terms of transmission error (shaded areas) obtained by numerical simulations using VSA when sweeping over a broad range of dimensionless profile depth E^* and extent Γ, for no lead crown and a lead crown of maximum amplitude according to the proposed theory ($B^*=1$). The curves corresponding to the analytical formulae (30) and (32) have been superimposed and it can be noticed that they

gear	A	B	C
α_0 (°)	20	20	25
β_0 (°)	19.5	14.7	13
z_1 ; z_2	25 ; 33	23 ; 33	35 ; 68
m_0 (mm)	12	10	2.5
b(mm)	180	100	40
ε_α	1.56	1.56	1.15
ε_β	1.59	0.81	1.39
x_1 , x_2	0.14 ; 0.03	0 ; 0.03	0.275 ; 0.317
δ_m (µm)	14.2	23.4	17.4
ha_1 ; ha_2	1.1 ; 1.1	1 ; 1	0.976 ; 0.970
hf_1 ; hf_2	1.25 ; 1.25	1.25 ; 1.25	1.262 ; 1.268
ρ	0.4	0.4	0.25
η(ε_β)	-0.235	0.399	-0.80

Table 1 – Gear data

agree well with the area of minimum TE_S time-variation amplitudes as found by the software code. It can be also verified that, depending on gear geometry, the presence of a lead crown

displaces the optimum area towards the smaller (Fig. 7) or larger (Fig. 8) relief amplitudes. The analytical formulae capture this effect and it is confirmed that $B^{*}\eta\left(\varepsilon_{\beta}\right)$ (and its sign) is crucial with regard to crowning contribution.

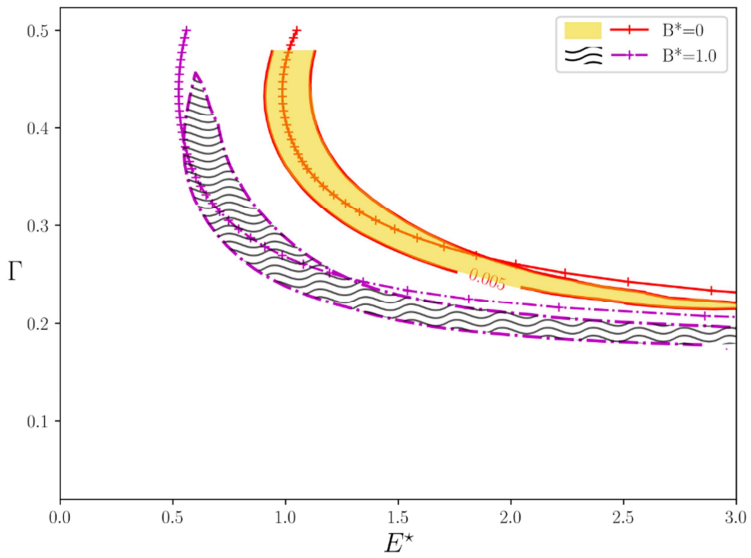

Figure 7 – Comparisons between (30), (32) (the two lines) and the optimum profile reliefs obtained by numerical sweeps using VSA (the shaded areas) for no crown and a crown amplitude equal to the average mesh deflection. Gear A in Table 1.

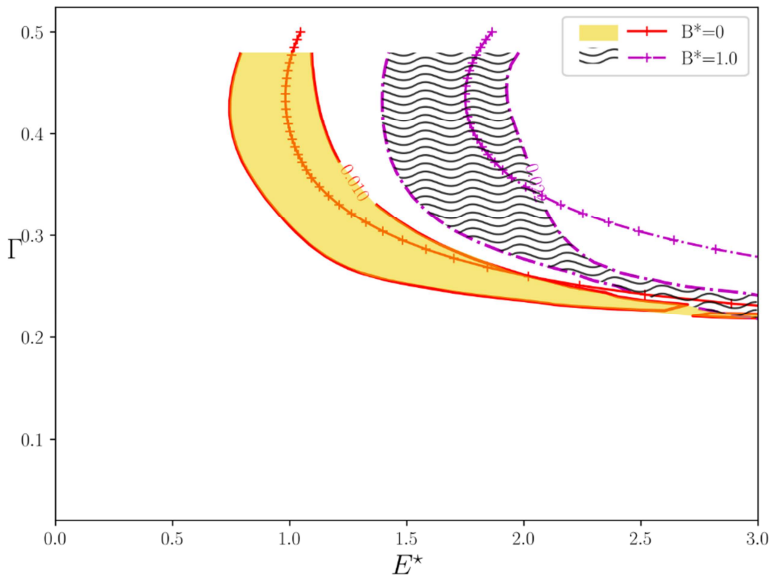

Figure 8 – Comparisons between (30), (32) (the two lines) and the optimum profile reliefs obtained by numerical sweeps using VSA (the shaded areas) for no crown and a crown amplitude equal to the average mesh deflection. Gear B in Table 1.

4-2 Hydrid model results:

The pinion and gear shaft geometry are described in Figure 9-a whereas gear data can be found in Table 1 (gear C). Three-dimensional brick finite elements are used to simulate the structural parts (Figure 9-b) and lumped stiffness elements represent the bearings (shaded on the FE grid). The finite element models of the pinion and gear shafts are condensed and connected by a time-varying non-linear Winkler foundation along with two mortar interfaces in order to avoid compatibility problems between the continuous and discrete models at play [30].

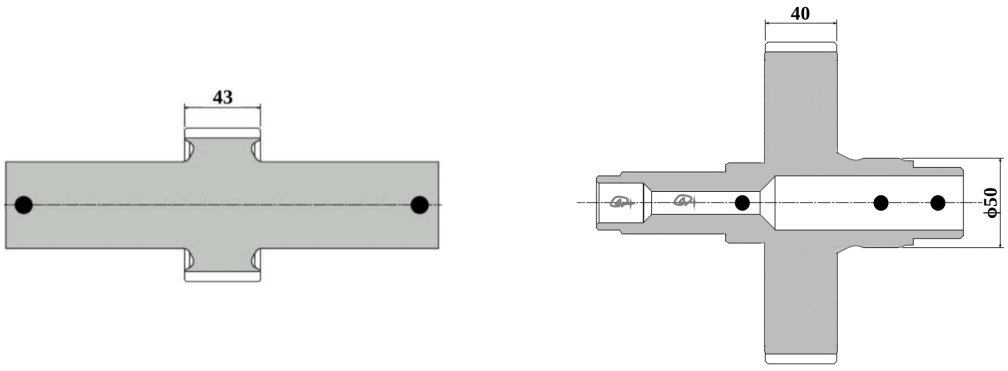

a)

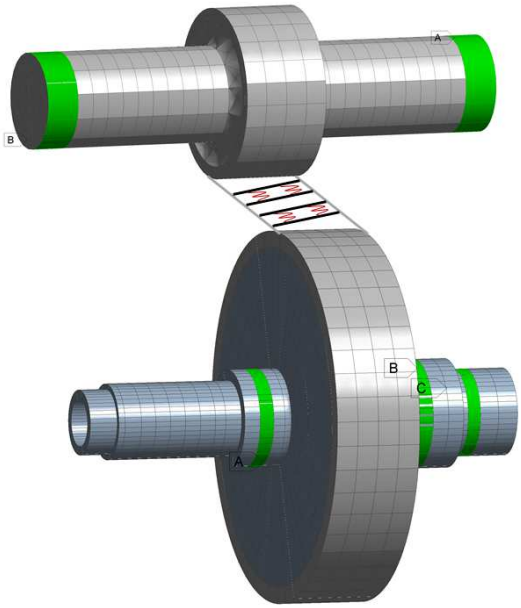

b)

Figure 9: Hybrid model: a) pinion and gear geometry, b) FE model and bearing locations.

A first series of simulations similar to those with VSA has been performed and the corresponding transmission error level curves are plotted in Figure 10. The curves representing the analytical formulae are superimposed and, here again, a good agreement is observed. Some complementary results are shown in Figure 11 where the length of profile

modification Γ is kept constant while the lead crown and relief amplitudes are varied. Examining the structure of (30) and (32), it is found that the optimum set of parameters should lie along a straight line in the $\left(E^*, B^*\right)$ plane. This finding is confirmed in Figure 11 where the minimum RMS zones derived from numerical sweeps are reasonably centred on the straight line deduced from (30) and (32). Similar results have already been found in [18].

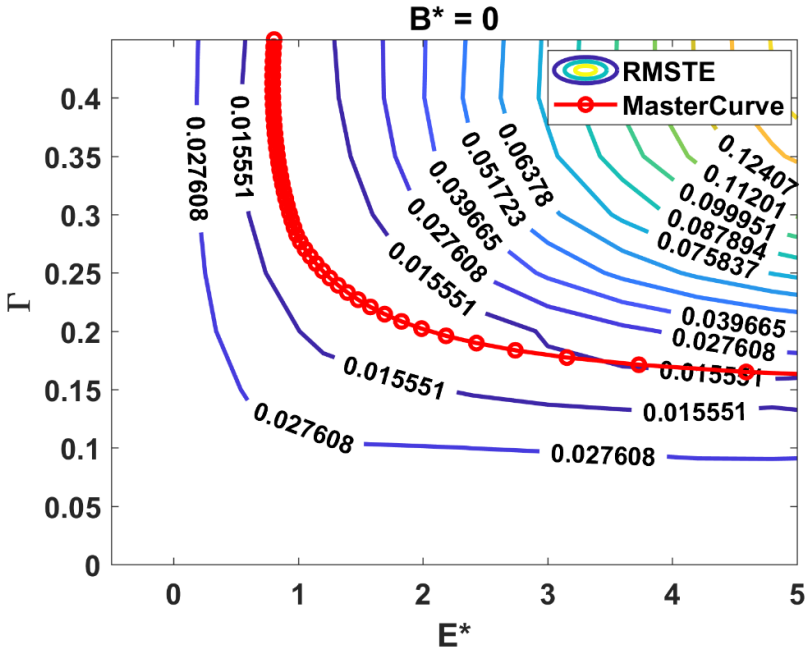

a)

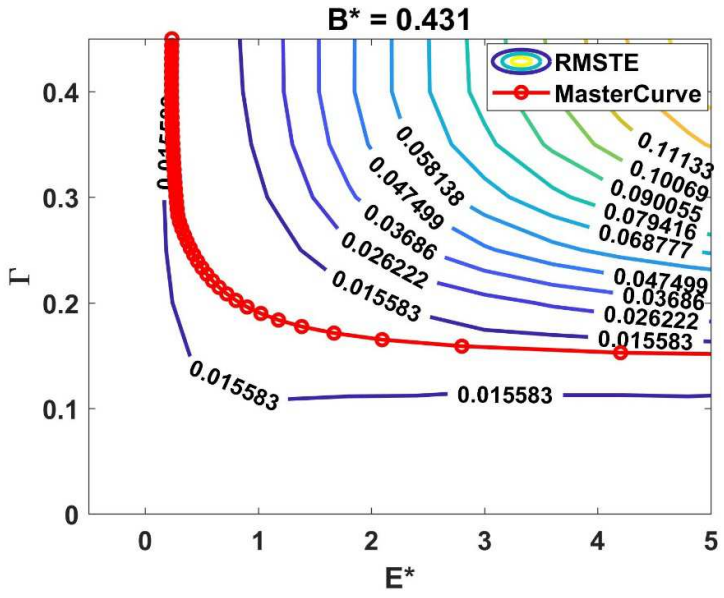

b)

Figure 10: Comparisons between the TE_S level curves obtained by using the hybrid model and the analytical results with a) no lead crown and, b) a moderate crown amplitude. Gear C in Table 1.

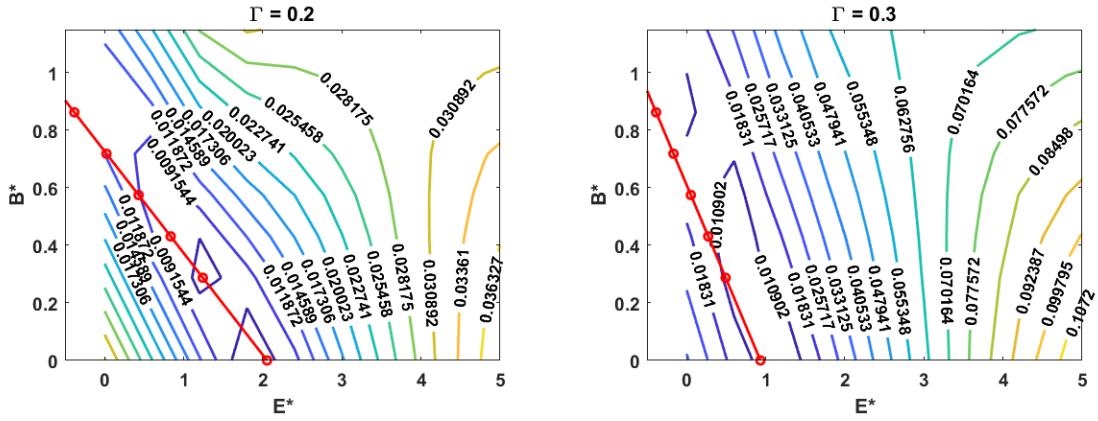

Figure 11: Comparisons between the TE_S level curves obtained by using the hybrid model and the analytical results. Representation in the (E^*, B^*) plane for two different extents of profile modification. Gear C in Table 1.

4-3 Comparisons with LDP results:

The main interest of this final set of comparisons stems from the elastic mesh interface model used in LDP, which is totally different from that in VSA and the Hybrid Model. A variable thickness plate model is employed for the structural deflections of the teeth and the contact algorithm is based on influence coefficients instead of distributed lumped stiffness elements, as is the case in VSA but also in the analytical approach in this paper. Two different gear geometries have been considered and results in line with those in the previous sections are presented. Figures 12 and 13 display the level curves of the RMS of transmission error as calculated by LDP along with the curves for the optimum tooth modifications based on (30) and (32). It can be observed that, here too, the analytical curves are near the numerical optimum. The comparisons are extended by keeping the extents of profile modifications constant and varying the relief and lead crown amplitudes (as in section 4-2). The results in Figures 14 and 15 clearly show that a very good agreement is obtained for a broad range of tooth modification parameters and that the analytical results are able to predict that no optimum shape modifications can be found for certain gear geometries.

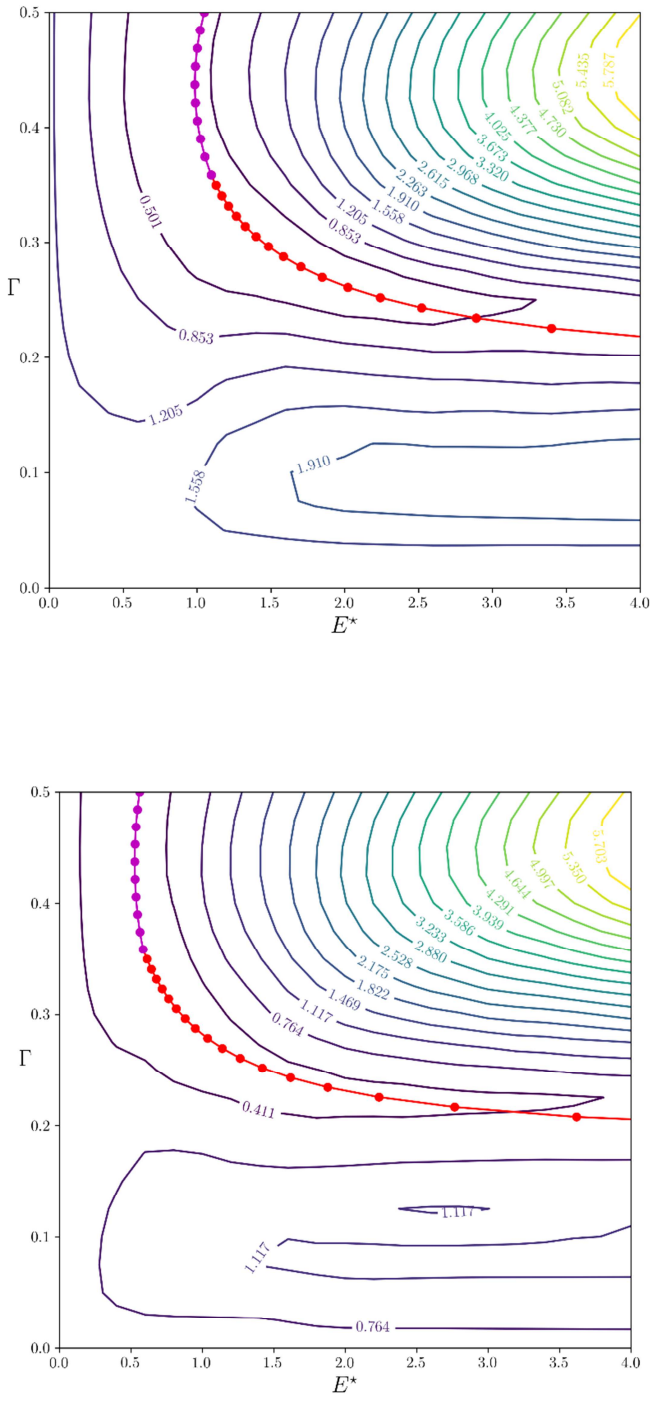

Figure 12 – Comparisons between the TE_S level curves obtained by using LDP and the analytical results with a) no lead crown and, b) a crown amplitude B^* =1- Gear A in Table 1

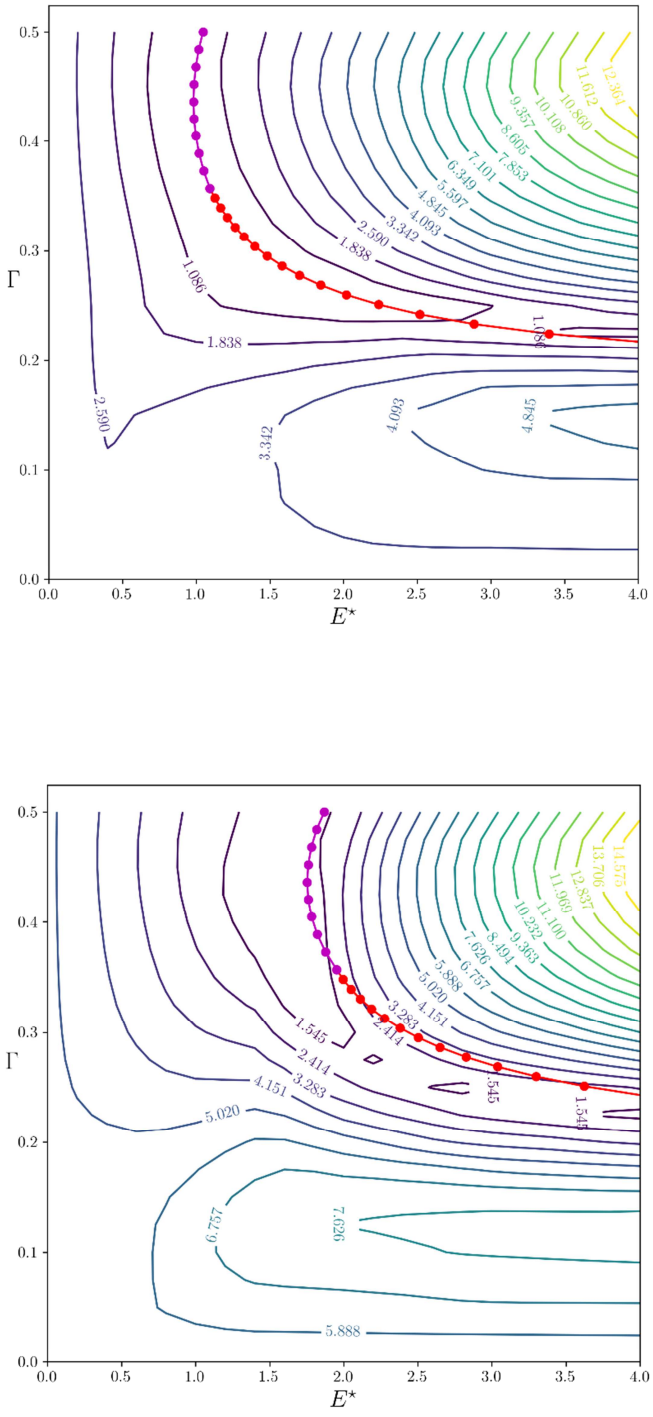

Figure 13 – Comparisons between the TE_S level curves obtained by using LDP and the analytical results with a) no lead crown and, b) a crown amplitude B^* =1- Gear B in Table 1

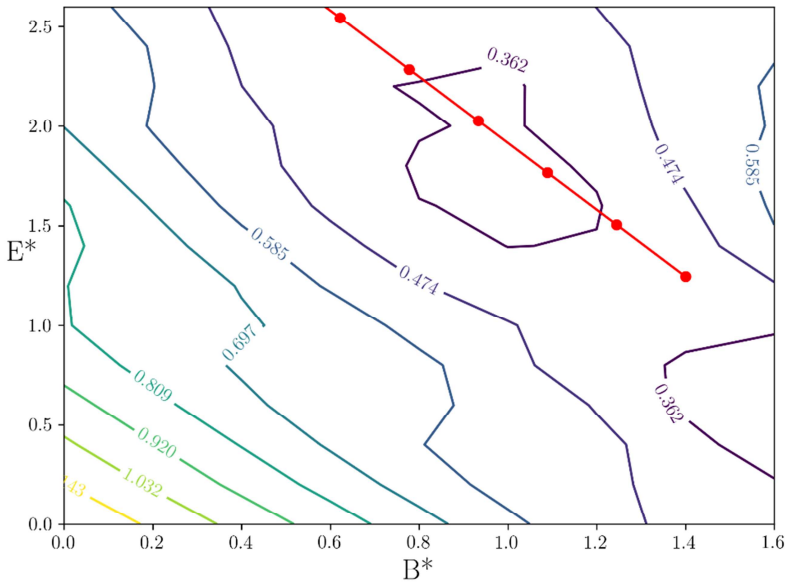

a) $\Gamma = 0.2$

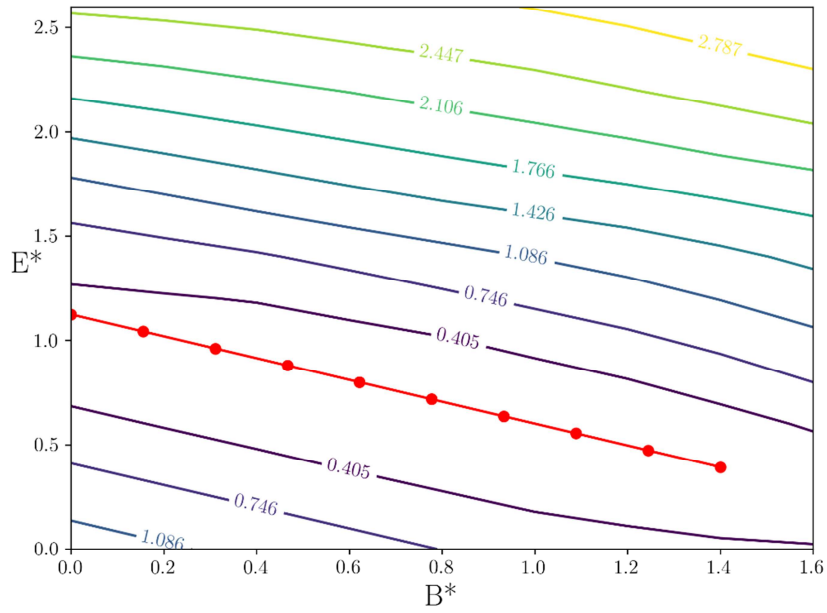

b) $\Gamma = 0.35$

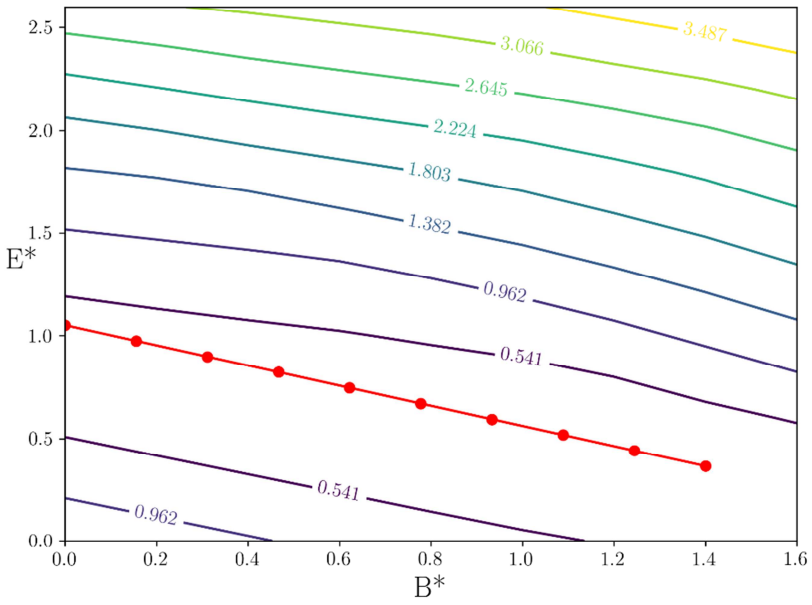

c) $\Gamma = 0.5$

Figure 14 – Comparisons between the TE_S level curves obtained by using LDP and the analytical results (30) and (32). Representation in the $\left(E^*, B^*\right)$ plane for different extents of profile modification. Gear A in Table 1.

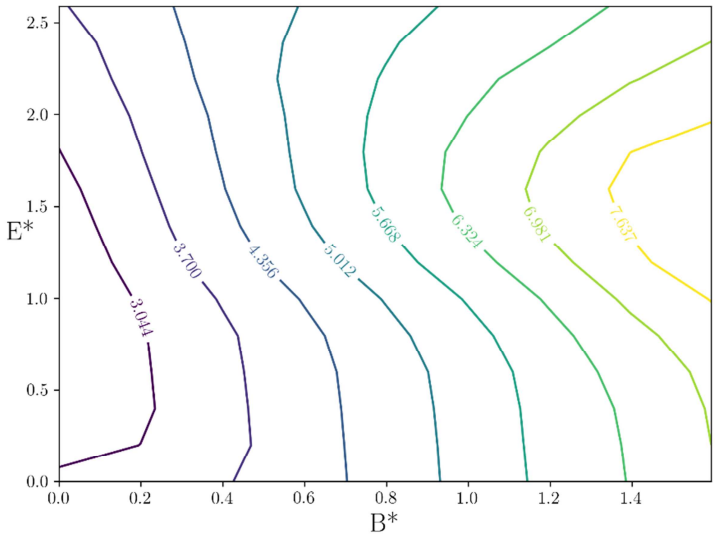

a) $\Gamma = 0.25$

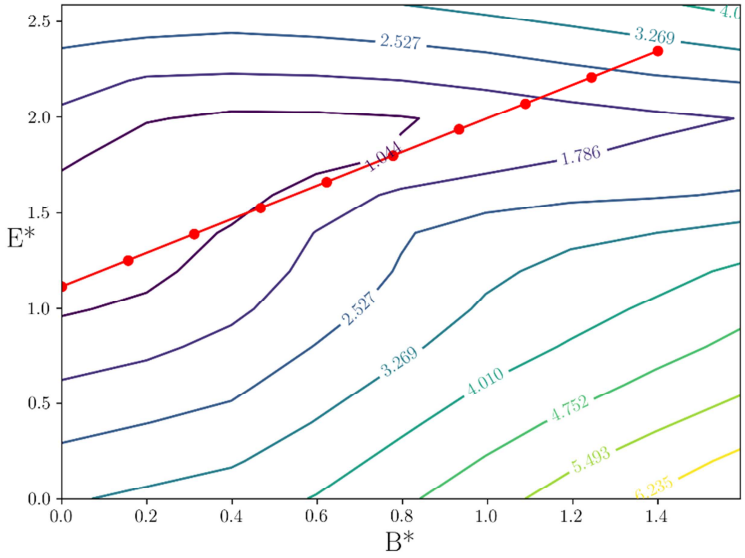

b) $\Gamma = 0.35$

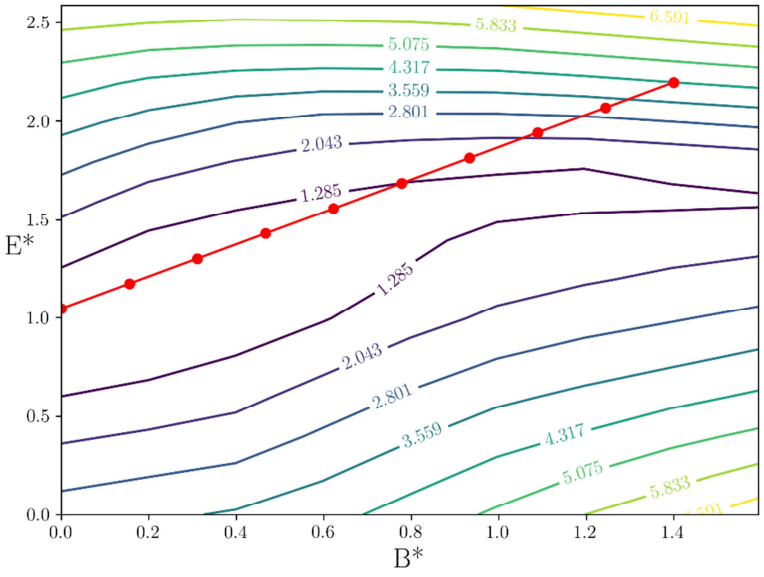

c) $\Gamma = 0.5$

Figure 15 – Comparisons between the TE_S level curves obtained by using LDP and the analytical results (30) and (32). Representation in the (E^*, B^*) plane for different extents of profile modification. Gear B in Table 1.

Conclusion

An original analytical approach has been presented which leads to closed-form expressions for the optimum tooth shape modifications minimising transmission error in narrow-faced helical gears. The theory is limited to symmetric linear profile relief combined with parabolic lead crown of moderate amplitude, i.e., such that the actual contact width remains close to the theoretical one. The analytical results are consistent with the previous formulae derived for profile relief only [25-27] since they have similar structures and only differ by a correcting term proportional to lead crown amplitude. Extensive comparisons with several software code results based on various mesh interface models show that the proposed formulae agree well with numerical predictions over a broad range of gear geometry and load, thus validating the proposed analytical findings. From a fundamental viewpoint, it is found that the contribution of lead crown is largely controlled by a particular function of the face contact ratio (Figure 5), which can be positive, negative or nil depending on gear geometry. The corresponding optimum shape modifications therefore exhibit contrasted sensitivity to lead crown and, in some cases, can be virtually independent of it. Interestingly, the analytical results point to a simple linear relationship between the optimum relief and crown amplitudes if the extent of profile modification is kept constant. The numerical results by two different models confirm this finding. It is also confirmed that, for errorless gears with integral face contact ratios, the introduction of lead crown can only be detrimental with regard to

transmission error. Because of their general character, it is believed that the analytical results presented in this paper might help shed light on the definition of the influential geometrical parameters on transmission error and therefore be useful at the early design stage. The proposed formulae can also generate initial solutions for more advanced numerical simulations, which can be required for thin-webbed or wide-faced gears for instance. Developments are currently under way to introduce parabolic profile modifications and investigate further the shape modifications minimising transmission error in relation to the notion of equivalent contact ratio as suggested in [20] for instance. Finally, beyond transmission error and load distribution, tooth shape modifications are known to have an impact on gear efficiency [37-39] and wear [40-41]; analytical investigations in these areas (in line with [27] for instance) on the specific contributions of combined profile and lead modifications would therefore be interesting extensions of the present work.

References :

[1] H. Walker, Gear tooth deflection and profile modification, The Engineer 166 (1938) 409-412.
[2] H. Walker, Gear tooth deflection and profile modification, The Engineer 170 (1940) 102-104.
[3] R.W. Gregory, S.L. Harris, R.G. Munro, Dynamic behaviour of spur gears, Proceedings of the Institution of Mechanical Engineers, 178 (1963) 207–226.
[4] G. Niemann, J. Baethge, Transmission error, tooth stiffness, and noise of parallel axis gears, VDI-Z, 112 (4) (1970) 205–276
[5] A. Kubo, K. Yamada, T. Aida and S. Sato, Research on ultra-high speed gear devices. Bull. JSME, 38 (1972) 2692-2715.
[6] H. N. Özgüven and D.R. Houser, Mathematical models used in gear dynamics—A review, Journal of Sound and Vibration, 121(3) (1988) 383-411. DOI: 10.1016/S0022-460X(88)80365-1.
[7] A. Kahraman and R. Singh, Non-linear dynamics of a spur gear pair, Journal of Sound and Vibration 142(1) (1990) 49-75. DOI: 10.1016/0022-460X(90)90582-K
[8] P. Velex, M. Maatar, A mathematical model for analyzing the influence of shape deviations and mounting errors on gear dynamic behaviour, Journal of Sound and Vibration 191 (5) (1996) 629–660.
[9] Y. Terauchi, H. Nadano, M. Nohara, On the effect of the tooth profile modification on the dynamic load and the sound level of a spur gear", Bull. JSME, 25 (207) (1982) 1474- 1481.
[10] T. Sato, K. Umezawa, J. Ishikawa, Effects of contact ratio and profile correction on gear rotational vibration, Bull. JSME, 26(221) (1983) 2010–2016.
[11] M.S. Tavakoli, D.R. Houser, Optimum profile modifications for the minimization of static transmission errors of spur gears, Journal of Mechanisms, Transmissions and Automation in Design 108 (1986) 86–95.
[12] R.G. Munro, N. Yildirim, D.L. Hall, Optimum profile relief and transmission error in spur gears, Proc. Int. Conf. on Gearbox noise and vibration, (1990) 35-42.
[13] N. Yildirim, R.G. Munro, A systematic approach to profile relief design of low and high contact ratio spur gears, Proc. IMechE, Part C, J. Mech. Eng. Science, 123 (C1) (1990) 551-562.
[14] C. Lee, H.H. Lin, F.B. Oswald, D.P. Townsend, Influence of Linear Profile Modification and Loading Conditions on The Dynamic Tooth Load and Stress of High-Contact-Ratio Spur Gears, J. Mech. Des. 113 (4) (1991) 473-480.

[15] Y. Cai, T. Hayashi, The optimum modification of tooth profile for a pair of spur gears to make its rotational vibration equal zero, Proc. 6th ASME Int. Power Trans. Gearing Conf., Phoenix, USA 1992, 453–460.
[16] H. H. Lin, F. B. Oswald, D. P. Townsend, Dynamic loading of spur gears with linear or parabolic tooth profile modifications, Mechanism and Machine Theory, 29 (8) (1994) 1115-1129.
[17] S. Matsumura, K. Umezawa, H. Houjoh, Performance diagram of a helical gear pair having tooth surface deviation during transmission on light load, Proc. 7th ASME Int. Power Trans. Gearing Conf., San Diego, USA 1996, 161–168.
[18] M. Maatar, P. Velex, Quasi-static and dynamic analysis of narrow-faced helical gears with profile and lead modifications, Journal of Mechanical Design 119 (4) (1997) 474–480.
[19] A. Kahraman, G.W. Blankenship, Effect of involute tip relief on dynamic response of gear pairs, Journal of Mechanical Design 121 (2) (1999) 313-315.
[20] E. N. Mohamad, M. Komori, H. Murakami, A. Kubo, S. Fang, Analysis of General Characteristics of Transmission Error of Gears With Convex Modification of Tooth Flank Form Considering Elastic Deformation Under Load, Journal of Mechanical Design, 131 (6) (2009) 061015, 9 pages.
[21] D.J. Fonseca, S. Shishoo, T.C. Lim, D.S. Chen, A genetic algorithm approach to minimize transmission error of automotive spur gear sets, Applied Artificial Intelligence, 19 (2) (2005), pp. 153-179, DOI: 10.1088/08839510590901903
[22] D. Ghribi, J. Bruyère, P. Velex, M. Octrue, M. Haddar, A contribution to the design of robust profile modifications in spur and helical gears by combining analytical results and numerical simulations, Journal of Mechanical Design 134 (6) (2012) 9 pages, DOI: 10.1115/1.4006740.
[23] G. Bonori, M. Barbieri, F. Pellicano, Optimum profile modifications of spur gears by means of genetic algorithms, Journal of Sound and Vibration, 133 (3-5),(2018), pp. 603-616.
[24] J.A. Korta, D. Mundo, Multi-objective micro-geometry optimization of gear tooth supported by response surface methodology, Mechanism and Machine Theory, 109 (2017), pp. 278-295, DOI: 10.1016/j.mechmachtheory.2016.11.015
[25] P. Velex, J. Bruyère, D.R. Houser, Some analytical results on transmission errors in narrow-faced spur and helical gears – Influence of profile modifications, Journal of Mechanical Design 133 (3) (2011), 11 pages, DOI: 10.1115/1.4003578.
[26] J. Bruyère, P. Velex, Derivation of optimum profile modifications in narrow-faced spur and helical gears using a perturbation method, Journal of Mechanical Design 135 (7) (2013), 8 pages, DOI: 10.1115/1.4024374.
[27] J. Bruyère, P. Velex, A simplified multi-objective analysis of optimum profile modifications in spur and helical gears, Mechanism and Machine theory, 80(1) (2014) 70-83, DOI: 10.1016/j.mechmachtheory.2014.04.015
[28] W. D. Mark, Tooth-meshing-harmonic static-transmission-error amplitudes of helical gears, Mechanical Systems and Signal Processing, 98 (2018) 506-533, DOI : 10.1016/j.ymssp.2017.04.039
[29] B. Guilbert, P. Velex, D. Dureisseix and P. Cutuli, A Mortar-based mesh interface for hybrid finite element / lumped parameter gear dynamic models – Applications to thin-rimmed geared systems, Journal of Mechanical Design, 138 (2016) 11 pages, DOI: 10.1115/1.4034220
[30] B. Guilbert, P. Velex, D. Dureisseix and P. Cutuli, Modular hybrid models to simulate the static and dynamic behaviour of high-speed thin-rimmed gears, Journal of Sound and Vibration, 438 (2019) 353-380.
[31] Weber, C., and Banaschek, K., 1953, *Formänderung und Profilrücknahme bei Gerad- und Schrägverzahnten Antriebstechnik*, Vieweg, Braunschweig, Vol. 11.

[32] D. R. Houser, J. Harianto, N. Iyer, J. Josephson and B. Chandrasekaren, , A multi-variable approach to determining the ‘best’ gear design, Proc. 8th ASME International Power Transmission and Gearing Conference, Baltimore, Sept. 2000, 8 pages.
[33] S. Sundaresan, K. Ishii, and D. R. Houser, A Procedure Using Manufacturing Variance to Design Gears With Minimum Transmission Error, Journal of Mechanical Design 113 (3) (1991) 318-325.
[34] S.Sundaresan, K. Ishii, D.R. Houser, Design Optimization for Robustness Using Performance Simulation Programs, Engineering Optimization 20(3) (1992) 163-178. DOI: 10.1080/03052159208941278
[35] S. Baud, P. Velex, Static and dynamic tooth loading in spur and helical geared systems – Experiments and model validation, Journal of Mechanical Design, 124 (2) (2002) 334-346.
[36] D. R. Houser, V. M. Bolze, J. M. Graber, A Comparison of Predicted and Measured Dynamic and Static Transmission Error for Spur and Helical Gear Sets, Proceedings of the 14th International Modal Analysis Conference, February 1996, 1057-1062, ISBN: 9780912053493 [0912053496]
[37] P. Velex, F. Ville, An Analytical Approach to Tooth Friction Losses in Spur and Helical Gears—Influence of Profile Modifications, Journal of Mechanical Design, 131(10) (2009) 10 pages. DOI:10.1115/1.3179156
[38] A. Diez-Ibarbia, A. Fernandez-del-Rincon, A. de-Juan, M. Iglesias, P. Garcia, F. Viadero, Frictional power losses on spur gears with tip reliefs. The load sharing role, Mechanism and Machine Theory, 112 (2017) 240-254. DOI: 10.1016/j.mechmachtheory.2017.02.012
[39] A. Diez-Ibarbia, A. Fernandez-del-Rincon, A. de-Juan, M. Iglesias, P. Garcia, F. Viadero, Frictional power losses on spur gears with tip reliefs. The friction coefficient role, Mechanism and Machine Theory, 121 (2018) 15-27. DOI:10.1016/j.mechmachtheory.2017.10.003
[40] F. Karpat, S. Ekwaro-Osire, Influence of tip relief modification on the wear of spur gears with asymmetric teeth, Tribology Transactions, 51(5) (2008) 581-588. DOI: 10.1080/10402000802011703
[41] T. Osman, P. Velex, Static and dynamic simulations of mild abrasive wear in wide-faced solid spur and helical gears, Mechanism and Machine Theory, 45(6) (2010) 911-924 DOI: 10.1016/j.mechmachtheory.2010.01.003

Annex 1

It has been demonstrated [26] that the quasi-static force on one tooth at any potential point of contact can be expressed as:

$$\hat{F}\left(\tau, z^*\right) = \cos\beta_b TE_S^*\left(\tau\right) + e^*\left(\tau, z^*\right) \qquad \text{(I-1)}$$

where $TE_S^*\left(\tau\right)$ is the quasi-static transmission error and $e^*\left(\tau, z^*\right)$ represents the actual tooth shape normal at the point M of coordinates $\left(\tau, z^*\right)$ in the base plane.

$\hat{F}\left(\tau, z^*\right)$ strictly positive corresponds to an actual point of contact M whereas a negative value of this function implies that there is no contact at M.

The problem of finding the reduction in contact length is formulated as to find the particular position on the line of action $\tau^\Delta = \lambda\varepsilon_\alpha$ such that the average tooth force in the face width direction is nil, hence:

$$\int_0^1 \hat{F}\left(\tau^\Delta = \lambda\varepsilon_\alpha, z^*\right) dz^* = 0 \qquad \text{(I-2)}$$

Re-written as:

$$\cos\beta_b TE_S^*\left(\tau^\Delta\right) + e_E^*\left(\tau^\Delta\right) + \int_0^1 e_B^*\left(z^*\right) dz^* = 0 \qquad \text{(I-3)}$$

Introducing the analytical expressions of the profile and lead modifications (1) and (2) and assuming that $\lambda < \Gamma$ give:

$$\cos\beta_b TE_S^*\left(\tau^\Delta\right) - E^*\left(1 - \frac{\lambda}{\Gamma}\right) - \frac{B^*}{3} \leq 0 \qquad \text{(I-4)}$$

Injecting in (I-4) the following main order approximation of transmission error

$$\cos\beta_b TE_S^*\left(\tau^\Delta\right) \geq \frac{1 - I_{kE0} - I_{kB0}}{I_{k0}} = \frac{\Gamma + E^*\left(\Gamma - \lambda\right)^2}{\Gamma\left(1 - 2\lambda\right)} + \frac{B^*}{3} \qquad \text{(I-5)}$$

leads to the following quadratic equation:

$$\Gamma + E^* \left(\Gamma - \lambda\right)^2 + E^* \left(\lambda - \Gamma\right)\left(1 - 2\lambda\right) \approx 0 \qquad \text{(I-6)}$$

whose only physically acceptable solution in terms of contact length reduction $\left(\lambda < 0.5\right)$ is :

$$\lambda \approx \frac{1 - \sqrt{1 - 4\Gamma\left(1 - \Gamma - 1/E^*\right)}}{2} \qquad \text{(I-7)}$$

which gives an approximate analytical expression of the contact length reduction.

Annex 2:

Consider two 1-periodic functions of the form:

$$\begin{aligned} f(\tau) &= f_0 + \Delta f(\tau) \\ g(\tau) &= g_0 + \Delta g(\tau) \end{aligned} \qquad \text{(II-1)}$$

with

$$\Delta f(\tau) = \sum_k a_k \cos\left(\pi k\left(2\tau - \varepsilon_\alpha - \varepsilon_\beta\right)\right)$$
$$\Delta g(\tau) = \sum_k b_k \cos\left(\pi k\left(2\tau - \varepsilon_\alpha - \varepsilon_\beta\right)\right)$$

The following equalities can be derived ($E(\bullet)$ *represents the average of a function*):

$$\begin{aligned} E\left(f(\tau)\right) &= f_0 \\ E\left(g(\tau)\right) &= g_0 \\ E\left(f(\tau) + g(\tau)\right) &= f_0 + g_0 \\ E\left(\Delta f(\tau)\right) &= E\left(\Delta g(\tau)\right) = 0 \end{aligned} \qquad \text{(II-2)}$$

Using Parseval's theorem, one obtains:

$$\begin{aligned} E\left(f^2(\tau)\right) &= f_0^2 + \frac{1}{2}\sum_k a_k^2 \\ E\left(g^2(\tau)\right) &= g_0^2 + \frac{1}{2}\sum_k b_k^2 \\ E\left(\left(f(\tau) + g(\tau)\right)^2\right) &= \left(f_0 + g_0\right)^2 + \frac{1}{2}\sum_k \left(a_k + b_k\right)^2 \end{aligned} \qquad \text{(II-3)}$$

From which, the variances of functions *f*, *g* and *f*+*g* can be derived as:

$$\begin{aligned} \mathrm{var}\left(f(\tau)\right) &= E\left(f^2(\tau)\right) - f_0^2 = \frac{1}{2}\sum_k a_k^2 \\ \mathrm{var}\left(g(\tau)\right) &= E\left(g^2(\tau)\right) - g_0^2 = \frac{1}{2}\sum_k b_k^2 \\ \mathrm{var}\left(f(\tau) + g(\tau)\right) &= \frac{1}{2}\sum_k \left(a_k + b_k\right)^2 \end{aligned} \qquad \text{(II-4)}$$

Assuming that the varying parts $\Delta f(\tau)$ and $\Delta g(\tau)$ are small compared with their averages f_0 and g_0, the ratio $\rho(\tau)=\frac{f(\tau)}{g(\tau)}$ can be approximated by using a first order Taylor's expansion of the form:

$$\begin{aligned}\rho(\tau) &\approx \left[\rho(\tau)\right]_{(f_0,g_0)} + \Delta f(\tau)\left[\frac{\partial\rho(\tau)}{\partial f}\right]_{(f_0,g_0)} + \Delta g(\tau)\left[\frac{\partial\rho(\tau)}{\partial g}\right]_{(f_0,g_0)} \\ &\approx \frac{f_0}{g_0} + \frac{\Delta f(\tau)}{g_0} - \frac{\Delta g(\tau)\, f_0}{g_0^2}\end{aligned} \tag{II-5}$$

the variance can be expressed as:

$$\begin{aligned}\mathrm{var}\left(\rho(\tau)\right) &= E\left(\left(\rho(\tau)-E\left(\rho(\tau)\right)\right)^2\right) \\ &\approx E\left(\left(\frac{\Delta f(\tau)}{g_0}-\frac{\Delta g(\tau)\, f_0}{g_0^2}\right)^2\right) \\ &\approx \frac{1}{g_0^2}E\left(\Delta f^2(\tau)\right)+\frac{f_0^2}{g_0^4}E\left(\Delta g^2(\tau)\right)-2\frac{f_0}{g_0^3}E\left(\Delta f(\tau)\Delta g(\tau)\right)\end{aligned} \tag{II-6}$$

The following relationships are used:

$$E\left(\Delta f^2(\tau)\right)=\mathrm{var}\left(\Delta f(\tau)\right)+\left[E\left(\Delta f(\tau)\right)\right]^2=\mathrm{var}\left(\Delta f(\tau)\right)=\mathrm{var}\left(f(\tau)\right)=\frac{1}{2}\sum_k a_k^2 \tag{II-7}$$

and the corresponding expressions for function *g*,

along with:

$$\begin{aligned}2E\left(\Delta f(\tau)\Delta g(\tau)\right) &= 2\,\mathrm{cov}\left(f(\tau),g(\tau)\right) \\ &= \mathrm{var}\left(f(\tau)+g(\tau)\right)-\mathrm{var}\left(f(\tau)\right)-\mathrm{var}\left(g(\tau)\right) \\ &= \frac{1}{2}\sum_k\left(a_k+b_k\right)^2-\frac{1}{2}\sum_k a_k^2-\frac{1}{2}\sum_k b_k^2 \\ &= \frac{1}{2}\sum_k\left[\left(a_k+b_k\right)^2-a_k^2-b_k^2\right] \\ &= \sum_k a_k b_k\end{aligned} \tag{II-8}$$

The variance of the ratio $\rho(\tau)=\frac{f(\tau)}{g(\tau)}$ can be approximated by:

$$\begin{aligned}\mathrm{var}\left(\rho(\tau)\right) &\approx \frac{1}{2g_0^2}\sum_k a_k^2+\frac{f_0^2}{2g_0^4}\sum_k b_k^2-\frac{f_0}{g_0^3}\sum_k a_k b_k \\ &\approx \frac{1}{2}\sum_k\left(\frac{a_k}{g_0}-\frac{f_0}{g_0^2}b_k\right)^2\end{aligned} \qquad \text{(II-9)}$$

Considering the case of transmission error, Eq. (5)-(10) lead to the following closed-form expressions:

$$\begin{aligned} f_0 &= 1+\frac{E^*\left(\Gamma-\lambda\right)^2}{\Gamma}+\frac{B^*}{3}\left(1-2\lambda\right) \\ g_0 &= \left(1-2\lambda\right) \\ a_k &= -\frac{E^*\left(\Gamma-\lambda\right)^2}{\Gamma}\Omega_{kE}+B^*\left(1-2\lambda\right)\Omega_{kB} \\ b_k &= \left(1-2\lambda\right)\Omega_k \end{aligned} \qquad \text{(II-10)}$$

which, combined with (II-9), finally gives the variance of transmission error as defined in (4) under the form:

$$\mathrm{var}\left(\cos\beta_b\, TE_S^*\right) \approx \frac{1}{2\left(1-2\lambda\right)^2}\sum_k\left(\Omega_k\left(1+\frac{E^*\left(\Gamma-\lambda\right)^2}{\Gamma}+\frac{\left(1-2\lambda\right)B^*}{3}\right)+\frac{E^*\left(\Gamma-\lambda\right)^2}{\Gamma}\Omega_{kE}-\left(1-2\lambda\right)B^*\Omega_{kB}\right)^2 \qquad \text{(II-11)}$$